Long-wave Marangoni convection in a thin film heated from below

S. Shklyaev,[1,2] A. A. Alabuzhev,[3,4] and M. Khenner[5]

[1]*Department of Chemical Engineering, California Institute of Technology, 1200 California Boulevard, Pasadena, California 91125, USA*

[2]*Department of Chemical Engineering, University of Puerto Rico–Mayagüez, Mayagüez, Puerto Rico 00681, USA*

[3]*Institute of Continuous Media Mechanics, Ural Branch of the Russian Academy of Sciences, Perm 614013, Russia*

[4]*Department of Theoretical Physics, Perm State University, 15 Bukirev Street, Perm 614990, Russia*

[5]*Department of Mathematics, Western Kentucky University, 1906 College Heights Boulevard, Bowling Green, Kentucky 42101, USA*

(Received 6 September 2011; revised manuscript received 28 November 2011; published 31 January 2012)

We consider long-wave Marangoni convection in a liquid layer atop a substrate of low thermal conductivity, heated from below. We demonstrate that the critical perturbations are materialized at the wave number $K \sim \sqrt{\mathrm{Bi}}$, where Bi is the Biot number which characterizes the weak heat flux from the free surface. In addition to the conventional monotonic mode, a novel oscillatory mode is found. Applying the $K \sim \sqrt{\mathrm{Bi}}$ scaling, we derive a new set of amplitude equations. Pattern selection on square and hexagonal lattices shows that supercritical branching is possible. A large variety of *stable* patterns is found for both modes of instability. Finite-amplitude one-dimensional solutions of the set, corresponding to either steady or traveling rolls, are studied numerically; a complicated sequence of bifurcations is found in the former case. The emergence of an oscillatory mode in the case of heating from below and stable patterns with finite-amplitude surface deformation are shown in this system for the first time.

DOI: 10.1103/PhysRevE.85.016328 PACS number(s): 47.55.pf, 47.54.−r, 47.20.Ky, 47.20.Dr

I. INTRODUCTION

Thermocapillary convection in a layer has been the focus of keen interest for more than 50 years. In the pioneering work by Pearson [1] two types of solid substrates were considered: an ideally thermally conductive one (in which case, the temperature of a liquid is fixed at the substrate) and a substrate of a very low conductivity (when a normal component of the heat flux is fixed at the substrate). The latter case is often called "insulated for perturbations substrate" in the literature. The long-wave instability mode is critical in this case for the zero value of the heat flux at the free surface (equivalently, the surface Biot number is zero). Later, this analysis was extended by including the surface deformation [2] and from the analysis a zero critical Marangoni number emerged (a value that does not depend on the other parameters of the system). Smith [3] pointed out that this unlikely result stems from the disregard of gravity by the authors of Ref. [2], and he obtained the correct formula for the two-layer system. The summary of other developments can be found in the survey [4] and in the monographs [5–7].

An especially important and thoroughly studied question is the emergence of an oscillatory mode in this system. For a conductive substrate, Takashima showed that oscillatory instability is possible only for heating from above (in reality, a cooling of a substrate instead of its heating) [8]. The paper by Birikh *et al.* [9] is devoted to a careful numerical analysis of the linear stability problem for both types of the thermal boundary conditions at the substrate; they found only the monotonic mode for heating from below.

Another important aspect is the nonlinear evolution of the system. The amplitude equation governing the long-wave Marangoni convection for a nondeformable free surface was obtained and studied by Knobloch [10] for infinite values of the Prandtl number and was soon corrected for finite values of this number [11]. The analysis of pattern selection for the latter case and for more general situations (including the second layer and weak interface deformation) was carried out in Ref. [12].

Many papers were devoted to the *long-wave* Marangoni convection in a layer with deformable free surface, see Refs. [13,14]. For the *conductive substrate*, a subcritical bifurcation takes place and film rupture occurs, which was evidenced within the direct numerical simulations of the Navier-Stokes equations [15], within the lubrication approximation [16–18], and experimentally [18]. Recent work [19] demonstrated that a fractal structure of droplets emerges as the result of evolution.

In the case of the substrate *insulated for perturbations*, the case we are dealing with, gravity usually is assumed sufficiently high [12], leading to the "slaved" surface deformation, which means that most of the nonlinear terms are the same as in the case when the free surface is nondeformable [10,11]. This restriction works well for a thin layer (with a thickness of $\sim$0.3 mm and larger for water), but fails for an ultrathin film. The only paper free of this limitation is by Garcia-Ybarra *et al.* [20], where a generalized Kuramoto-Sivashinsky equation for the film thickness was derived. (However, it must be noted that the account of the buoyancy effect is incorrect in their paper.) Interestingly, they showed that the supercritical excitation of rolls is possible when gravity is weak (i.e., for the Galileo number smaller than 45). However, since the authors assumed from the beginning of the analysis that the relative surface deformation was small (weakly nonlinear regime) the question whether the stable state with the *finite-amplitude* deflection of the free surface is possible remains unsolved. Moreover, they did not perform a more intricate analysis of three-dimensional patterns.

To summarize, common to all cited and other published studies is the following observation: (i) the oscillatory mode is found only when heating is from above, and (ii) when heating is from below, the film usually ruptures (i.e., there is no stable state with a finite deformation of a free surface). In this paper, we show the emergence of both phenomena for heating from below, which is certainly very important from a practical standpoint. Stable deformed states of a surface

with finite-amplitude deformation can be used, for instance, to localize dispersed particles, and the oscillatory mode, when it leads to the development of a traveling wave (see Secs. IV B and V B) can be used to transport drugs or chemical reagents across the substrate.

Importantly, the majority of papers devoted to the long-wave Marangoni convection in a layer atop a substrate of low thermal conductivity deal with the standard asymptotics $K \sim \mathrm{Bi}^{1/4}$, where K is the wave number of a perturbation and Bi is the Biot number of the free surface. However, as demonstrated by the authors of Ref. [21], in certain situations the conventional scaling becomes insufficient and the critical perturbation is materialized at a smaller wave number $K \sim \sqrt{\mathrm{Bi}}$. To the best of our knowledge the latter scaling was used only for the thermal convection in binary mixtures [21,22]. This scaling is central to our analysis, which details and extends the recent communication [23] by providing a thorough discussion of the linear stability problem, a weakly nonlinear analysis in a wider range of parameters, and studies of the two-dimensional regimes for finite nonlinearity.

The paper is organized as follows. In Sec. II we derive a set of amplitude equations which govern the coupled evolution of the layer thickness and the averaged (across the layer) part of the temperature. In Sec. III the linear stability analysis is performed; both monotonic and oscillatory instability modes are demonstrated. Section IV is devoted to the weakly nonlinear analysis on square and hexagonal lattices. In Sec. V we study the nonlinear evolution of two-dimensional regimes; steady and traveling rolls are considered. Conclusions are drawn in Sec. VI.

II. AMPLITUDE EQUATIONS

A. Problem statement

We consider a three-dimensional thin liquid film of the unperturbed height H on a planar horizontal substrate heated from below. The thermal conductivity of the solid is assumed small in comparison with the one of the liquid so that the constant vertical temperature gradient $-A$ is prescribed in a liquid at the contact with the substrate. The Cartesian reference frame is chosen such that the x and y axes are in the substrate plane and the z axis is normal to the substrate.

We use H^2/χ, H, χ/H, $\rho\nu\chi H^{-2}$, and AH as the units for the time, the length, the velocity, the pressure, and the temperature, respectively. (Here χ is the thermal diffusivity, ν is the kinematic viscosity, and ρ is the density of the liquid.) This results in the following dimensionless boundary-value problem:

$$\nabla\cdot\mathbf{v} = 0, \tag{1a}$$

$$\frac{1}{\mathrm{Pr}}\left(\mathbf{v}_t + \mathbf{v}\cdot\nabla\mathbf{v}\right) = -\nabla p + \nabla^2\mathbf{v} - G\mathbf{k}, \tag{1b}$$

$$T_t + \mathbf{v}\cdot\nabla T = \nabla^2 T, \tag{1c}$$

$$\mathbf{v} = 0, \quad T_z = -1 \quad \text{at} \quad z = 0,$$

$$h_t = w - \mathbf{v}\cdot\nabla h, \quad p = \mathrm{Ca}\nabla\cdot\mathbf{n} + \mathbf{n}\cdot\sigma\cdot\mathbf{n}, \tag{2a}$$

$$\mathbf{t}\cdot\sigma\cdot\mathbf{n} = -M\mathbf{t}\cdot\nabla\left(T|_{z=h}\right),$$

$$\mathbf{n}\cdot\nabla T = -\mathrm{Bi}\,T \quad \text{at} \quad z = h(x,y,t). \tag{2b}$$

Here $\mathbf{v} = (\mathbf{u}, w)$ is the fluid velocity ($\mathbf{u}$ is velocity in the substrate plane and w is the vertical component), T is the temperature, p is the pressure in the liquid, σ is the viscous stress tensor, h is the dimensionless height of the film, $\mathbf{k}$ is the unit vector directed along the z axis, $\mathbf{n} = (\mathbf{k} - \nabla h)/\sqrt{1 + (\nabla h)^2}$ is the normal unit vector to the free surface, $\mathbf{t}$ is the tangent vector; a superscript denotes the corresponding derivative. The problem is characterized by the following dimensionless parameters:

$$\mathrm{Ca} = \frac{\sigma_0 H}{\rho\nu\chi}, \quad M = -\frac{\sigma_T A H^2}{\rho\nu\chi}, \quad G = \frac{g_0 H^3}{\nu\chi},$$
$$\mathrm{Bi} = \frac{qH}{\kappa}, \quad \mathrm{Pr} = \frac{\nu}{\chi},$$

which are the capillary number, the Marangoni number, the Galileo number, the Biot number, and the Prandtl number, respectively. Here σ_0 is the surface tension, $\sigma_T \equiv d\sigma_0/dT$, q is the heat transfer coefficient, and κ is the thermal conductivity.

Equations (1) and (2) have an obvious base solution, which corresponds to the conductive state

$$h^{(0)} = 1, \quad T^{(0)} = -z + \frac{1+\mathrm{Bi}}{\mathrm{Bi}}, \quad p^{(0)} = G(1-z). \tag{3}$$

Below we study the stability of this solution with respect to long-wave perturbations and the evolution of the large-scale perturbations to the conductive state. It is worth noting that formally $T^{(0)}$ diverges at $\mathrm{Bi} = 0$. This fact has an obvious physical explanation: Writing the heat losses in Eq. (2b) in the form $-\mathrm{Bi}T$ means that the temperature of the gas far from the film is a reference value. In view of the smallness of the heat flux from the free surface, the film temperature has to be rather high, thus resulting in the $O(\mathrm{Bi}^{-1})$ term.

B. Lubrication approximation

To study the evolution of large-scale flows, we rescale the coordinates, the time, and the velocity according to the relations

$$X = \epsilon x, \quad Y = \epsilon y, Z = z, \quad \tau = \epsilon^2 t, \quad \mathbf{u} = \epsilon\mathbf{U}, \quad w = \epsilon^2 W, \tag{4}$$

where $\epsilon \ll 1$ can be thought of as the ratio of H to a typical horizontal lengthscale.

Then we expand all the fields in a power series with respect to ϵ^2

$$\mathbf{U} = \mathbf{U}_0 + \epsilon^2\mathbf{U} + \cdots, \quad W = W_0 + \epsilon^2 W_1 + \cdots,$$
$$p = p_0 + \epsilon^2 p_1 + \cdots, \tag{5}$$
$$T = -z + \mathrm{Bi}^{-1} + T_0 + \epsilon^2 T_1 + \cdots.$$

We do not write an expansion for h for the sake of brevity. Indeed, on one hand we are interested in regimes with the finite-amplitude surface deformation; the slow variation of h, ensured by Eq. (4), is sufficient to provide a small-amplitude motion [13,14]. On the other hand, small corrections to the leading order for h are unimportant for further analysis.

The perturbations of the temperature and pressure are not required to be small as well; however, the perturbation gradients must be small. Also, we note that we do not drop out the equilibrium fields, Eq. (3), from T and p; indeed,

comparing Eqs. (3) and (5), it becomes obvious that the base conductive state corresponds to $T_0 = 1,\ p_0 = p^{(0)}$.

Finally, we assume large values of Ca and a small Biot number

$$\mathrm{Ca} = \epsilon^{-2} C, \quad \mathrm{Bi} = \epsilon^2 \beta. \tag{6}$$

As noted in Sec. I, the scaling for the Biot number differs from the conventional $\mathrm{Bi} = O(\epsilon^4)$ [13,20]. In fact, this means that we deal with the smaller values of the wave number than those implied by the usual scaling.[1]

Both scalings, Eq. (6), are important for our analysis, as will be made clear in Sec. III. The capillary number is often assumed large for the ideally thermally conductive substrate [13,18], but in the case under consideration (the substrate of a low conductivity) $\mathrm{Ca} = O(1)$ is usually set [20,21]. We do not make this assumption. Moreover, very often the Galileo number is taken as large [12], the assumption that is justified for thin layers, $H > 0.3$ mm for water, but fails for ultrathin films. We do not impose restrictions on the magnitude of the Galileo number.

Substituting Eqs. (4)–(6) into Eqs. (1) and (2) we obtain in the zero order

$$W_{0Z} = -\nabla \cdot \mathbf{U}_0, \quad p_{0Z} = -G, \tag{7a}$$

$$\mathbf{U}_{0ZZ} = \nabla p_0, \quad T_{0ZZ} = 0, \tag{7b}$$

$$\mathbf{U}_0 = W_0 = T_{0Z} = 0 \quad \text{at} \quad Z = 0, \tag{7c}$$

$$p_0 = -C\nabla^2 h, \quad h_\tau = -\mathbf{U}_0 \cdot \nabla h + W_0,$$

$$T_{0Z} = 0, \quad \mathbf{U}_{0Z} = -M\nabla(T_0 - h) \quad \text{at} \quad Z = h. \tag{7d}$$

Hereafter $\nabla \equiv (\partial_X, \partial_Y, 0)$ is a two-dimensional projection of the gradient operator onto the X-Y plane.

The solution to this boundary value problem is

$$p_0 = \Pi(X,Y,\tau) - GZ, \quad T_0 = \theta(X,Y,\tau), \tag{8a}$$

$$\mathbf{U}_0 = \tfrac{1}{2} Z(Z - 2h)\nabla\Pi - MZ\nabla f, \tag{8b}$$

$$W_0 = \frac{Z^2}{2}\nabla \cdot \left[\frac{1}{3}(3h - Z)\nabla\Pi + M\nabla f\right], \tag{8c}$$

where $\Pi = Gh - C\nabla^2 h$ and $f = \theta - h$ has a meaning of perturbation of the free surface temperature (in other words, $-f$ is the surface tension perturbation). The evolution of the layer thickness is governed by the well-known condition $h_\tau = -\nabla \cdot \int_0^h \mathbf{U}_0 \mathrm{d}Z$, which provides the first amplitude equation

$$h_\tau = \nabla \cdot \left(\frac{h^3}{3}\nabla\Pi + \frac{Mh^2}{2}\nabla f\right) = \nabla \cdot \mathbf{j}. \tag{9}$$

The vector $-\mathbf{j}$ has a meaning of the longitudinal flux of a liquid averaged across the layer. This flux vanishes in the simplest situation [i.e., for the steady one-dimensional (1D) case], but in general it is nonzero (for instance, for time-periodic regimes).

To obtain the second amplitude equation we proceed to the first order of the expansion, where we need only the heat transfer equation

$$T_{1ZZ} = \theta_\tau - \nabla^2\theta + \mathbf{U}_0 \cdot \nabla\theta - W_0, \tag{10a}$$

$$T_{1Z} = 0 \text{ at } Z = 0, \tag{10b}$$

$$T_{1Z} = \nabla\theta \cdot \nabla h - \tfrac{1}{2}(\nabla h)^2 - \beta f \quad \text{at} \quad Z = h. \tag{10c}$$

The solvability condition of this problem is obtained by the integration of Eq. (10a), while accounting for the boundary conditions. This results in

$$h\theta_\tau = \nabla \cdot (h\nabla\theta) - \frac{1}{2}(\nabla h)^2 - \beta f + \mathbf{j} \cdot \nabla f + \nabla \cdot \left(\frac{h^4}{8}\nabla\Pi + \frac{Mh^3}{6}\nabla f\right). \tag{11}$$

Accounting for Eq. (9) one can rewrite Eq. (11) as follows:

$$h\left(f + \frac{5h}{8}\right)_\tau = \nabla \cdot (h\nabla\theta) - \frac{1}{2}(\nabla h)^2 + \mathbf{j} \cdot \nabla\left(f + \frac{3}{8}h\right) - \beta f - \frac{M}{48}\nabla \cdot (h^3\nabla f), \tag{12}$$

which is sometimes convenient.

Equations (9) and (11) form a closed set of amplitude equations, which governs the nonlinear dynamics of long-wave perturbations. These equations include the following effects: in the right-hand side of Eq. (9), damping of the surface deflection due to gravity and surface tension, and influence of the thermocapillary flow on the layer thickness; in the right-hand side of Eq. (11), heat conductivity in the longitudinal directions (the first term), heat losses from the free surface [the second and third terms, where the second term describes the effect originating from the increase of the surface area (at constant volume)], and advective heat transfer by the flow (the fourth and fifth terms).

The base state, corresponding to motionless fluid [see Eq. (8)] with a constant heat flux maintained through the layer, is given by $h = \theta = 1$.

To the best of our knowledge this set of amplitude equations is new. Most papers deal with the limiting case $\beta = 0$, which, in particular, corresponds to the conventional asymptotics $K \sim \mathrm{Bi}^{1/4}$. [To develop correctly the conventional asymptotics one has to add the $\beta_2\epsilon^4$ term in Eq. (6) and take the $O(\epsilon^4)$ terms into account.] Among the other works, this limiting case was studied in Ref. [20] within the 1D problem and under the assumption of small perturbations of h and θ. Thus at $\beta = 0$ we expect that the results of Ref. [20] must be reproduced, see Secs. III B and IV A.

It is noteworthy that the set of Eqs. (9) and (11) is reminiscent of the sets of nonlinear amplitude equations derived by the author of Refs. [24,25]. The first paper dealt with the Marangoni convection in a layer of a binary liquid for a finite Biot number; the Galileo and Lewis numbers were assumed small, which resulted in the finite contribution of the surface tension in the long-wave dynamics. The second paper described the buoyancy convection in a two-layer system with a deformable interface under assumption of large Ca. The oscillatory mode for this system was found in Ref. [26];

[1] To find critical perturbations one has to consider all possible values of the wave number. Usually, $K \sim \sqrt{\mathrm{Bi}}$ results in trivial results and conventional scaling is enough to determine the global minimum of the neutral stability curve. However, there are few examples where the intermediate asymptotics, materialized by Eq. (6), is needed (see, for instance, Ref. [21]).

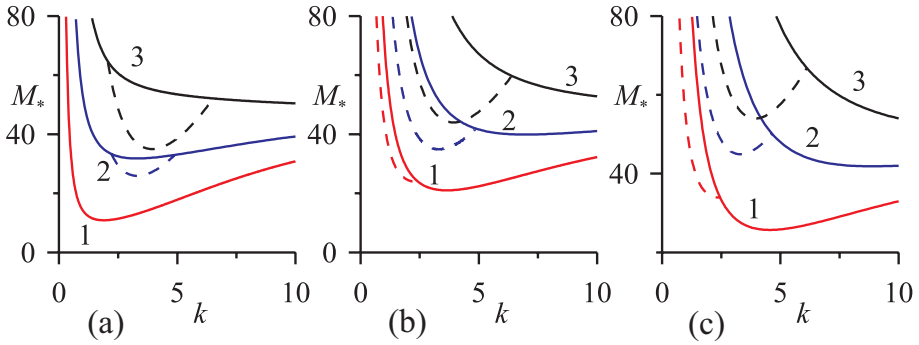

FIG. 1. (Color online) Marginal stability curves $M_*(k)$. The solid lines correspond to the monotonic mode, $M_m(k)$, the dashed ones to the oscillatory mode $M_o(k)$; $\beta = 10, 40, 80$ for lines 1, 2, and 3, respectively. (a) $G = 1$, (b) $G = 10$, (c) $G = 20$.

the surface-tension-driven convection was accounted for in Ref. [27].

III. LINEAR STABILITY ANALYSIS

A. Dispersion relation

Substituting the perturbed fields $h = 1 + \xi$ and $\theta = 1 + \Theta$ into Eqs. (9) and (11) and linearizing the equations for perturbations about the equilibrium, one arrives at

$$\xi_\tau = \nabla^2\left[\frac{1}{3}(G\xi - C\nabla^2\xi) + \frac{M}{2}(\Theta - \xi)\right], \tag{13a}$$

$$\Theta_\tau = \nabla^2\left[\Theta + \frac{1}{8}(G\xi - C\nabla^2\xi) + \frac{M}{6}(\Theta - \xi)\right] - \beta(\Theta - \xi). \tag{13b}$$

Representing the perturbation fields proportional to $\exp(\lambda\tau + ikX)$ gives the quadratic equation for the growth rate

$$\lambda^2 + \lambda\left[\beta + k^2\left(1 + \frac{\tilde{G} - M}{3}\right)\right] + \frac{k^2}{3}(\beta + k^2)\tilde{G} - \frac{Mk^4}{2}\left(1 + \frac{\tilde{G}}{72}\right) = 0, \tag{14}$$

where $\tilde{G} \equiv G + Ck^2$. Equation (14) possesses both real (monotonic instability) and complex (oscillatory instability) solutions.

The instability modes governed by Eq. (14) have not been studied yet. As we noted above, the case $\beta = 0$ is often considered [1,6,20]. The only paper dealing with the case of finite β is the work of the authors of Ref. [21] (see Sec. IV there), where a binary liquid layer is considered for $C = 0$ (or equivalently, finite Ca). The matching in the common limiting case $C = 0$ in Eq. (14) and $\chi = 0$ (the absence of the Soret effect) in Eq. (B15) of the cited paper indeed takes place.

B. Monotonic mode

For the monotonic mode $\lambda = 0$ at the stability border, thus the neutral stability curve is given by

$$M_m = \frac{48(\beta + k^2)\tilde{G}}{k^2(72 + \tilde{G})}. \tag{15}$$

These neutral curves have a minimum at the finite values of k only if

$$\beta C < 72, \tag{16}$$

otherwise the minimum value $M_c^{(sw)} = 48$ is achieved in the limit $k \to \infty$ (i.e., the shortwave mode is critical). Holding inequality (16) true, we obtain $M_m < 48$. Recall that $M_c^{(sw)} = 48$ represents the critical value found by Pearson [1] for a nondeformable surface.

For $C = 0$ (Ca is finite) the critical Marangoni number reduces to the conventional value $M_m = 48G/(G + 72)$ found in Ref. [20]. Again, this minimum is approached for $k \to \infty$ at any finite β. The same result is valid for $\beta = 0$ as well, but the critical wave number is zero in this case. (Recall that this limiting case corresponds to the conventional scaling.)

Since we are not interested in the limiting case $C = 0$ any further, we set $C = 1$ hereafter, which is equivalent to choosing $\epsilon^2 = 1/\mathrm{Ca}$ in Eqs. (4) through (6). This, in particular, means that $\beta = \mathrm{BiCa}$ below.

The typical marginal stability curves for the monotonic mode are presented in Fig. 1.

The critical wave number materializing the minimum of the marginal stability curve, Eq. (15), is

$$\left(k_c^{(m)}\right)^2 = \frac{\beta G + \sqrt{72\beta G(G + 72 - \beta)}}{72 - \beta}. \tag{17}$$

The corresponding value of the critical Marangoni number is $M_c^{(m)} = M_m(k_c^{(m)})$. Note, that at $\beta \to 0$, the critical wave number is proportional to $\beta^{1/4}$, thus guaranteeing the matching with the conventional asymptotics. (See the detailed comparison in Sec. III D.)

The results of the minimization of the marginal stability curve with respect to k are shown in Fig. 2. It is clear that the growth of β leads to the layer stabilization ($M_c^{(m)}$ increases) due to either heat losses from the free surface or damping of

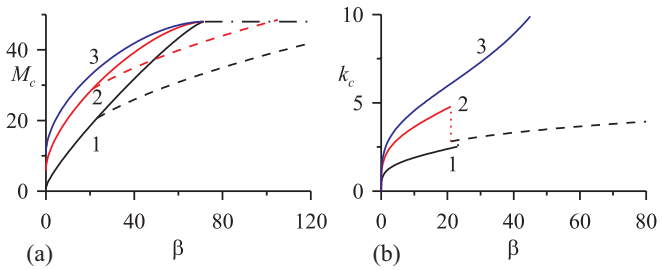

FIG. 2. (Color online) (a) Variation of the critical Marangoni number and (b) the critical wave number k_c with β. Solid lines correspond to the monotonic mode; dashed ones to the oscillatory mode. Dashed-dotted line in panel (a) displays the shortwave monotonic mode at $\beta > 72$, $M_c^{(sw)} = 48$. Lines 1, 2, and 3 correspond to $G = 1$, $G = 10$, and $G = 20$, respectively.

the surface deflection by surface tension. The critical wave number $k_c^{(m)}$ grows with the increase in β, tending to infinity at $\beta = 72$, when the shortwave mode sets in with $M_c^{(sw)} = 48$. In fact, the computation for a finite unscaled wave number $K = \epsilon k$, which is not presented here, shows that the critical Marangoni number for the shortwave mode at $\beta > 72$ slightly exceeds 48 and depends on G and each of Bi and Ca separately, rather than on β only. (Of course, with the growth of Bi the difference $M_c^{(sw)} - 48$ increases.) Thus, $M_c^{(sw)} = 48$ gives a reasonable stability threshold for the shortwave mode at small enough values of the Biot number and $\beta > 72$.

C. Oscillatory mode

For the oscillatory mode the marginal stability curve is determined by the expression

$$M_o = 3 + \frac{3\beta}{k^2} + G + k^2. \tag{18}$$

The imaginary part of the growth rate for neutral perturbations is

$$\lambda_i = \frac{k^2}{12}\sqrt{(72 + G + k^2)(M_m - M_o)}. \tag{19}$$

(Hereafter we use subscripts r and i to denote the real and imaginary parts of a complex value, respectively.) It is clear that the oscillatory mode is present only at $M_o(k) < M_m(k)$ (see Fig. 1). Examples of the marginal stability curves for this mode are shown in Fig. 1.

Minimizing the Marangoni number with respect to k we obtain

$$M_c^{(o)} = 3 + G + 2\sqrt{3\beta}, \quad k_c^{(o)} = (3\beta)^{1/4}. \tag{20}$$

The variation of both the critical Marangoni number and the critical wave number for the oscillatory mode with β is presented in Fig. 2. At $G < G_* = 17.16$, the oscillatory mode becomes critical at certain $\beta = \beta_1(G)$, see the dashed lines 1 and 2 branching from the corresponding solid lines in Fig. 2(a). The critical wave number is discontinuous at $\beta = \beta_1$, as demonstrated in Fig. 2(b), and $k_c^{(o)}$ becomes the critical wave number instead of $k_c^{(m)}$. Since the former function does not depend on G, each solid curve collapses to the single dashed line in Fig. 2(b) at $\beta = \beta_1$. With the further increase in β a monotonic mode again becomes critical at $\beta = \beta_2(G)$. This monotonic mode can be either long wave at $\beta_2 < 72$, or shortwave at $\beta_2 > 72$. In the latter case $\beta_2(G)$ is determined by the condition $G = 45 - 2\sqrt{3\beta_2}$. The parameter range where the novel oscillatory mode is critical is shown in Fig. 3.

D. Comparison with the previous studies

Keeping in mind the possible future attempts at the verification of our findings in the experiments and numerical simulations, below we state the expressions for the neutral stability curves in terms of the unscaled wave number $K = \epsilon k$, Biot number Bi and capillary number Ca. For the monotonic mode, the stability threshold is given by

$$M_m = 48\frac{(\mathrm{Bi} + K^2)(G + \mathrm{Ca}K^2)}{K^2(72 + G + \mathrm{Ca}K^2)}, \tag{21}$$

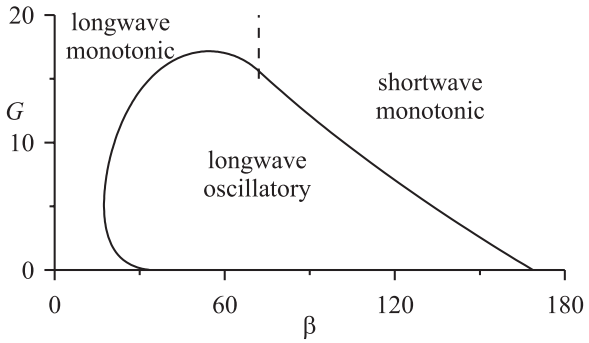

FIG. 3. The domain of oscillatory instability. The dashed vertical line marks the boundary of the long-wave monotonic instability, Eq. (16).

whereas for the oscillatory mode the stability threshold is

$$M_o = 3 + \frac{3\mathrm{Bi}}{K^2} + G + \mathrm{Ca}K^2. \tag{22}$$

(Recall that Bi and K are small, whereas Ca is large.)

As we have noted in Sec. III B, Eq. (21) reproduces two known asymptotics $M_m = 48$ for a nondeformable surface ($G + \mathrm{Ca}K^2 \gg 72$) at large K or $\mathrm{Bi} = 0$ [1], $M_m = 48G/(72 + G)$ at $\mathrm{Bi} = 0$ ($K_c = 0$ for the critical perturbation) [20]. Equation (22) has no known limits because the oscillatory convection for the heating from below is reported in this paper for the first time.

Another important issue behind Eqs. (21) and (22) is the explanation of the scalings given by Eq. (6). These scalings provide that (i) the heat diffusivity and heat flux from the free surface are comparable [the term $\mathrm{Bi} + K^2$ in Eq. (21) and the term $3 + 3\mathrm{Bi}K^{-2}$ in Eq. (22)] and (ii) contributions of the gravity and surface tension are of the same order of magnitude (the term $G + \mathrm{Ca}K^2$ in both equations).

For the monotonic mode one can demonstrate the connection between the case extensively studied earlier, $\mathrm{Bi} \ll K^2$, and the current analysis in terms of the above-mentioned competitions of the damping effects. Indeed, at $\mathrm{Bi} = 0$ the neutral stability curve is given by

$$M_m = 48\frac{G + \mathrm{Ca}K^2}{72 + G + \mathrm{Ca}K^2} \tag{23}$$

with the zero critical wave number, which diminishes the stabilizing effect of the surface tension. At small K, the neutral stability curve Eq. (23) is as follows:

$$M_m \approx \frac{48}{72 + G}\left(G + \frac{72}{72 + G}\mathrm{Ca}K^2\right).$$

It is evident that the heat loss at the free surface is most important for the long-wave perturbations with $K = 0$, when the contribution of thermal diffusivity is vanishingly small, Bi versus K^2 in the numerator of Eq. (21). Hence, for small Bi the wavelength of critical perturbations is determined by the balance of two stabilizing effects, the surface tension $\mathrm{Ca}K^2$ (most pronounced for larger K) and heat losses from the free surface $\mathrm{Bi}K^{-2}$ (most efficient for small K). This balance provides

$$K_c^4 \sim \frac{\mathrm{Bi}}{\mathrm{Ca}}, \tag{24}$$

which agrees with Eq. (17) at small β or its unscaled analog

$$K_c^2 = \sqrt{\frac{\mathrm{Bi}G(G+72)}{72\mathrm{Ca}}}. \tag{25}$$

For finite Ca Eq. (25) provides the conventional asymptotics $K_c \sim \mathrm{Bi}^{1/4}$. However, the increase in Ca leads to a strong stabilization of the convection owing to the surface tension and hence it makes the wavelength of critical perturbations smaller, ensuring the scalings given by Eqs. (4) and (6).

A similar simple qualitative explanation of the oscillatory mode emergence is not possible because all physical effects (the surface tension, heat losses, diffusion and advection of heat, etc.) are important for this mode. Hence there are no simple particular cases to be analyzed. However, Eq. (22) and Fig. 3 explain why the oscillatory mode has not been found earlier. As we had emphasized above, all previous studies deal with one of the following three cases: (i) the nondeformable surface $G \gg 1$, (ii) the case of extremely small heat losses $K^2 \gg \mathrm{Bi}$, (iii) the case of the weak surface tension effect $\mathrm{Ca} = O(1)$. Case (i) is of no interest since no oscillatory instability occurs at large G, see Fig. 3. In case (ii), $M_o > M_m$ irrespective of K, Ca, and G (i.e., the oscillatory mode does not exist). In case (iii), one obtains that the critical wave number for the oscillatory mode tends to infinity, thus leaving the domain of validity of the long-wave approximation. In other words, both cases (ii) and (iii) correspond to small $\beta = \mathrm{BiCa}$, whereas this product must be finite for the emergence of this novel oscillatory mode (see Fig. 3). Therefore only a delicate balance of the surface tension and heat losses $\mathrm{Bi} \sim \mathrm{Ca}^{-1} \sim K^2$ is able to capture the oscillatory perturbations.

Finalizing this section, we provide the estimate for a water layer of a thickness of 0.05 mm. This results in $G \approx 10$, $\mathrm{Ca} \approx 5 \cdot 10^4$; assuming $q = 10\,\mathrm{W/m^2K}$ one obtains $\mathrm{Bi} \approx 10^{-3}$. The characteristic wavelength of the convective structure is provided by $H/\sqrt{\mathrm{Bi}} \approx 2$ mm, whereas the period of oscillation can be estimated as $H^2/\nu\mathrm{Bi} \approx 3$ s. The critical Marangoni number is attained at the temperature difference 0.5 K. Therefore for such a layer the novel oscillatory mode can be found. Dealing with more viscous liquid one can increase the thickness of the layer.

IV. WEAKLY NONLINEAR ANALYSIS

Here we study the nonlinear dynamics of perturbations assuming small supercriticality $M \approx M_*(k)$. We do not specify the chosen wave number, but in the computations $k = k_c^{(m,o)}$ (and thus $M_* = M_c^{(m,o)}$) is set for the corresponding mode.

A. Monotonic mode

We present h, θ, M, and the time derivative as a power series in small δ, where δ is a measure of the supercriticality

$$h = 1 + \delta\xi_1 + \cdots, \quad \theta = 1 + \delta\Theta_1 + \cdots, \tag{26a}$$

$$M = M_m + \delta M_1 + \cdots, \quad \partial_\tau = \delta\partial_{\tau_1} + \delta^2\partial_{\tau_2} + \cdots. \tag{26b}$$

In the expansion of the time derivative, we have taken into account that for the monotonic mode the evolution is determined only by the nonlinear terms, quadratic (τ_1) or cubic (τ_2).

Substituting this ansatz into Eqs. (9) and (11), and collecting the terms of equal powers in δ, we obtain in the first order the linear stability problem, Eq. (13).

Its solution can be presented as

$$\xi_1 = \sum_{j=1}^{n} A_j(\tau_1,\tau_2)\exp(i\mathbf{k}_j\cdot\mathbf{R}) + \text{c.c.}, \tag{27a}$$

$$\Theta_1 = \alpha\sum_{j=1}^{n} A_j(\tau_1,\tau_2)\exp(i\mathbf{k}_j\cdot\mathbf{R}) + \text{c.c.}, \tag{27b}$$

where c.c. denotes complex conjugate terms, $\alpha = 1 - 2(G + k^2)/3M_m$ and $|\mathbf{k}_j| = k$. Below we carry out the calculations for two particular cases.

(i) Square lattice ($n = 2$):

$$\mathbf{k}_1 = k(1,0), \quad \mathbf{k}_2 = k(0,1).$$

(ii) Hexagonal lattice ($n = 3$):

$$\mathbf{k}_1 = k(1,0), \quad \mathbf{k}_2 = \tfrac{1}{2}k(-1,\sqrt{3}), \quad \mathbf{k}_3 = -\tfrac{1}{2}k(1,\sqrt{3}). \tag{28}$$

For the *square lattice*, in the second order we obtain the usual result $\partial_{\tau_1} = M_1 = 0$ [28]; the elimination of the secular terms in the third order leads to

$$\dot{A}_1 = (\gamma M_2 - K_0|A_1|^2 - K_1|A_2|^2)A_1, \tag{29}$$

$$\dot{A}_2 = (\gamma M_2 - K_0|A_2|^2 - K_1|A_1|^2)A_2, \tag{30}$$

where the dot denotes the derivative with respect to τ_2, $\gamma = d\lambda/dM > 0$, the self-interaction (K_0) and cross-interaction (K_1) coefficients are real. It is known [28] that two types of the steady solutions are possible.

Rolls $A_1 = \sqrt{\gamma M_2/K_0}$, $A_2 = 0$ branch supercritically at

$$K_0 > 0. \tag{31}$$

Squares $A_1 = A_2 = \sqrt{\gamma M_2/(K_0 + K_1)}$ emerge through the direct bifurcation at

$$K_0 + K_1 > 0. \tag{32}$$

Of course, if any of the conditions, Eqs. (31) or (32), are violated then both the rolls and squares become unstable near the stability threshold.

Pattern selection on the square lattice is governed by the difference of the self-interaction and the cross-interaction coefficients. Rolls are selected when the condition

$$K_1 > K_0 \tag{33}$$

is met. In the opposite case squares are stable on the square lattice.

Coefficients K_0 and K_1 are very cumbersome and therefore they are not given here. The domains of stability for rolls and squares are presented in Fig. 4. One can readily see that supercritical branching occurs only in two domains of the parameters. These domains are situated either at rather small values of β, Fig. 4(b), or at sufficiently small G, Fig. 4(c). In the first case rolls are selected except for a very small region shown in the inset. Conversely, in the second case squares are selected anywhere, excluding a small area, where rolls are stable. For $\beta = 0$ the domain of supercritical bifurcation for the rolls shown in Fig. 4(a) is limited by condition

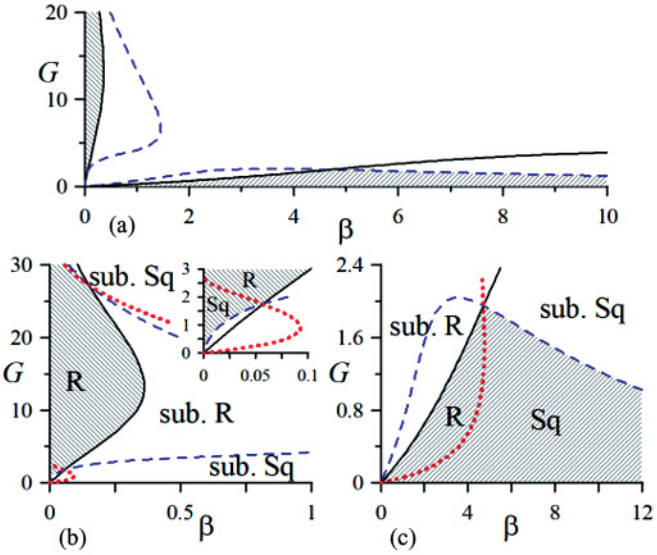

FIG. 4. (Color online) (a) The domains of stability (crosshatched) of patterns on the square lattice. Panels (b) and (c) show zoomed-in domains of stability for the rolls (marked with an "R") and squares ("Sq"). Solid (dashed) lines are the boundaries between regions of supercritical and subcritical branching for rolls (squares). The domains of subcriticality are marked by "sub. R" ("sub. Sq"). Dotted lines corresponding to $K_0 = K_1$, see Eq. (33), separate the domains of stable rolls and squares.

$G < 45$ in accordance with the result obtained by the authors of Ref. [20].

For the *hexagonal lattice*, resonant quadratic interaction results in the following system of the amplitude equations in the second order:

$$\partial_{\tau_1} A_1 = \gamma M_1 A_1 - N A_2^* A_3^*, \tag{34}$$

and the similar pair of equations, produced from Eq. (34) by the cyclic permutation of the subscripts. These equations describe the subcritical excitation of the hexagonal patterns through a transcritical bifurcation. The coefficient N is not of a fixed sign and it vanishes under the condition

$$(G + k^2)(3\beta + 2k^2) + 36(\beta - k^2) = 0, \text{ or } \beta = \beta_*(G). \tag{35}$$

The locus of points determined by Eq. (35) is shown in Fig. 5.

In the vicinity of this line, assuming $N \approx \delta N_1$, we should set $\partial_{\tau_1} = M_1 = 0$ and further (cubic) nonlinear terms are needed. Proceeding to the third order of expansion, we derive the set of equations

$$\dot{A}_1 = \gamma M_2 A_1 - N_1 A_2^* A_3^* - \left[K_0 A_1^2 + K_2\left(A_2^2 + A_3^2\right)\right] A_1, \tag{36}$$

and a similar pair of equations for $A_{2,3}$. Here again the dot denotes the derivative with respect to τ_2. Three among the variety of patterns are important for further analysis. They are rolls with $A_1 = \sqrt{\gamma M_2/K_0}$, $A_2 = A_3 = 0$ and two types of hexagons with $A_1 = A_2 = A_3 \equiv A$: H^+ for $A > 0$ and H^- in the opposite case. In the first case the flow is upward in the center of the convective cell, whereas in the second case it is downward.

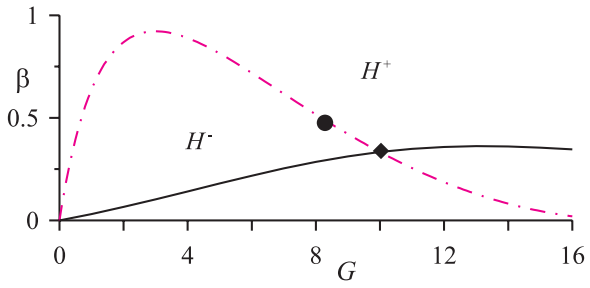

FIG. 5. (Color online) Pattern selection for the monotonic mode on a hexagonal lattice. Dashed-dotted line presents the locus of points $\beta = \beta_*(G)$, Eq. (35), where the quadratic term in Eq. (34) vanishes. Up (down) hexagons H^+ (H^-) emerge above (below) the line. Equation (36) is appropriate in the vicinity of this curve. Below the solid line $K_0 > 0$ [this line coincides with the solid line in Fig. 4(a)]. The circle ($G = G_1 \approx 8.20$) and diamond ($G = G_2 = 10$) separate domains of stability within Eq. (36): at $G < G_1$ no stable regimes exist near the stability threshold; at $G_1 < G < G_2$ stable Hexagons emerge when the condition given by Eq. (38) is satisfied; at $G > G_2$ Hexagons are stable at M_2 given by Eq. (38), whereas rolls are stable when Eq. (39) is satisfied.

An analysis of this set of amplitude equations was carried out in Refs. [29,30]. There it was shown that the parameter

$$\tilde{a} \equiv \frac{K_2}{K_0 - K_2} \tag{37}$$

is determinative. (Hereafter we take into account the inequality $K_2 > K_0$, which holds true in the entire range of parameters.) The typical bifurcation diagrams when $\tilde{a}$ is varied are given, for instance, in Fig. 9 of Ref. [30]. At $\tilde{a} > -1/2$ ($G < G_1$, where G_1 is shown by the circle in Fig. 5) there is no stable solutions, and the subcritical bifurcation takes place for rolls and one branch of hexagons. If $-1 < \tilde{a} < -1/2$ ($G_1 < G < G_2$, where G_2 is shown by the diamond in Fig. 5), the rolls are still subcritical and unstable; stable hexagons (H^+ above the dashed-dotted line in Fig. 5 or H^- below the line) occur only within the finite interval of M_2

$$-\frac{N_1^2}{4(K_0 + 2K_2)} < \gamma M_2 < \frac{N_1^2 (2K_0 + K_2)}{(K_2 - K_0)^2}. \tag{38}$$

Finally, at $\tilde{a} < -1$ ($G > G_2$), one of the hexagons is stable within the interval defined by Eq. (38) and the rolls are stable when

$$\gamma M_2 > \frac{N_1^2 K_0}{(K_2 - K_0)^2}. \tag{39}$$

Concluding this section, we briefly discuss the competition of patterns belonging to the square and hexagonal lattices. First, it is clear that at finite values of N, hexagons emerge subcritically and no stable small-amplitude patterns can be found near the stability threshold. Therefore, patterns stable on the both lattices can be found only near the curve $\beta = \beta_*(G)$, shown in Fig. 5. However, this line intersects only the domain of stability for rolls, but not for squares. Therefore, squares

are always unstable and the selected patterns are either rolls or hexagons[2].

It is noteworthy that the pattern selection for the monotonic mode differs considerably from the results found for a nondeformable (or a slightly deformable) free surface ($\beta = 0, G \to \infty$) [12]. In the cited paper the following results were found. First, no stable rolls exist on a square lattice, only squares are selected. Second, the boundary separating the up and down hexagons depends on the Prandtl number only. Third, the competition between patterns on square and hexagonal lattices results in the emergence of squares at large M_2.

Another paper appropriate for a comparison is Ref. [31], where both buoyancy and thermocapillary convection in a layer with an upper nondeformable surface was studied for finite values of the Biot number. In this case the stability of rolls against the formation of squares (the mode termed as "cross-roll instability" there) is found as well. (In fact, the rolls are mentioned to be unstable within the pure Marangoni problem, but this instability is the "phase" one; either the Ekhaus or zigzag mode, which do not belong to the lattices under consideration.) Thus in some sense our problem (finite β or $K \sim \sqrt{\mathrm{Bi}}$) has more in common with the problem for finite Bi than with the problem for $K \sim \mathrm{Bi}^{1/4}$.

B. Oscillatory mode

For the oscillatory mode we repeat the procedure described in Sec. IV A. We supplement Eq. (26a) with

$$\partial_\tau = \partial_{\tau_0} + \delta^2 \partial_{\tau_2} + \cdots, \quad M = M_o + \delta^2 M_2 + \cdots, \tag{40}$$

separating the fast oscillation in τ_0 and the slow nonlinear evolution of the amplitude in τ_2. The first-order solution is represented in the form

$$\xi_1 = \sum_{j=1}^{n} A_j(\tau_2) \exp(i\mathbf{k}_j \cdot \mathbf{R} - i\omega\tau_0) + \text{c.c.}, \tag{41a}$$

$$\Theta_1 = \alpha_o \sum_{j=1}^{n} A_j(\tau_2) \exp(i\mathbf{k}_j \cdot \mathbf{R} - i\omega\tau_0) + \text{c.c.}, \tag{41b}$$

where $\omega = -\lambda_i$ and $\alpha_o = 1 - 2(G + k^2)/3M_o + 2i\omega/M_o k^2$ according to the linear stability theory. Calculating the expansion to the third order in δ, we arrive at conventional amplitude equations. We again deal with two types of lattices: the square and hexagonal ones.

For the *square lattice*, we represent ξ_1 as follows:

$$\xi_1 = (A_1 e^{ikX} + A_2 e^{-ikX} + B_1 e^{ikY} + B_2 e^{-ikY}) e^{-i\omega\tau_0} + \text{c.c.} \tag{42}$$

[2]Of course, squares can be found in a confined cavity, square in the horizontal plane, $0 < X, Y < \pi/k$ with adiabatic vertical walls, see the remark concerning the relation between periodic regimes and steady states in a confined geometry in Sec. V.

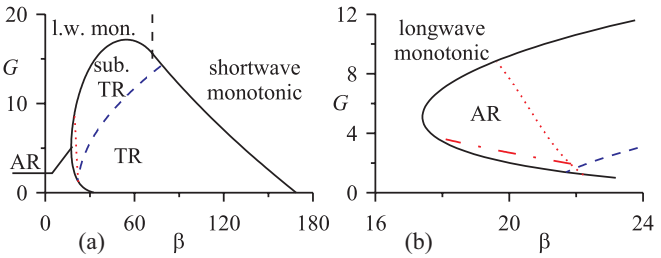

FIG. 6. (Color online) Selection of oscillatory patterns on a square lattice. (a) Domains of stability for TR (below the dashed line) and AR (to the left of the dotted line) are marked by "TR" and "AR," respectively. Above the dashed line TR bifurcate subcritically. (b) Zoomed in fragment of panel (a). AR are stable against perturbations belonging to a hexagonal lattice only below the dashed-dotted line.

The set of amplitude equations, which governs the dynamics of the amplitudes $A_{1,2}$ and $B_{1,2}$, reads

$$\dot{A}_1 = (\gamma M_2 - K_0|A_1|^2 - K_1|A_2|^2)A_1 - K_2(|B_1|^2 + |B_2|^2)A_1 - K_4 A_2^* B_1 B_2, \tag{43a}$$

$$\dot{A}_2 = big(\gamma M_2 - K_0|A_2|^2 - K_1|A_1|^2)A_2 - K_2(|B_1|^2 + |B_2|^2)A_2 - K_4 A_1^* B_1 B_2, \tag{43b}$$

and a similar pair of equations that obtained from Eqs. (43) by replacing A_j with B_j ($j = 1,2$) and vice versa. Hereafter the asterisk denotes the complex-conjugate term. The Landau coefficients K_l ($l = 0,1,2,4$) as well as the growth rate γM_2 are now complex-valued.

Equations (43) were studied in detail by the authors of Ref. [32]. They found six types of solutions.

(i) Traveling rolls (TR), $A_1 \neq 0$, $A_2 = B_1 = B_2 = 0$.
(ii) Standing rolls (SR), $A_1 = A_2 \neq 0$, $B_1 = B_2 = 0$.
(iii) Traveling squares (TS), $A_1 = B_1 \neq 0$, $A_2 = B_2 = 0$.
(iv) Standing squares (SS), $A_1 = A_2 = B_1 = B_2$.
(v) Alternating rolls (AR), $A_1 = A_2 = iB_1 = iB_2$.
(vi) Standing cross-rolls (SCR), $A_1 = A_2$, $B_1 = B_2$, $|A_1| \neq |B_1|$.

Using the results of the authors of Ref. [32], we have found that TR can branch either supercritically ($K_{0r} > 0$) or subcritically ($K_{0r} < 0$), whereas other patterns emerge through the direct Hopf bifurcation. The domains of supercritical and subcritical excitations for TR are demonstrated in Fig. 6(a).

A stability analysis for the patterns on the square lattice shows that TR are selected if they emerge through the direct Hopf bifurcation [see Fig. 6(a)]. In the opposite case the amplitude of TR grows to infinity and the system leaves the domain of validity of Eqs. (43). Alternating rolls are stable within the small area marked by "AR"; here depending on the initial condition the system either approaches AR or demonstrates the infinite growth of one of the amplitudes.

For the *hexagonal lattice*, it is convenient to rewrite Eqs. (41) in the form

$$\xi_1 = (A_1 e^{ikX} + A_2 e^{-ikX} + B_1 e^{i\mathbf{k}_2\cdot\mathbf{R}} + B_2 e^{-i\mathbf{k}_2\cdot\mathbf{R}} + C_1 e^{i\mathbf{k}_3\cdot\mathbf{R}} + C_2 e^{-i\mathbf{k}_3\cdot\mathbf{R}}) e^{-i\omega\tau_0} + \text{c.c.}, \tag{44}$$

where $\mathbf{k}_j$ given by Eq. (28) are the base wave vectors for the lattice.

The complex amplitudes A_j, B_j, and C_j are governed by the set of equations comprised of

$$\dot{A}_1 = (\gamma M_2 - K_0|A_1|^2 - K_1|A_2|^2 - \tilde{K}_2 S_1 - K_3 S_2)A_1 - \tilde{K}_4 A_2^*(B_1 B_2 + C_1 C_2), \quad (45a)$$

$$\dot{A}_2 = (\gamma M_2 - K_0|A_2|^2 - K_1|A_1|^2 - \tilde{K}_2 S_2 - K_3 S_1)A_1 - \tilde{K}_4 A_1^*(B_1 B_2 + C_1 C_2), \quad (45b)$$

plus the two similar pairs of equations, obtained from Eq. (45) by the cyclic permutation of A_j, B_j, and C_j. Here $S_j = |B_j|^2 + |C_j|^2 (j = 1,2)$,

An analysis of the Hopf bifurcation with the hexagonal symmetry was performed in Ref. [33], where 11 limit cycles were found. Six of them coincide with the above-mentioned solutions (i) through (v), but on a rhombic (in the Fourier space) lattice. They are TR, SR, traveling rectangles 1 and 2 (TRa1 and TRa2), standing rectangles (SRa), and alternating rolls on a rhombic lattice (AR-R). Obviously, two different types of TRa are possible, which are based, for example, on wave vectors $\mathbf{k}_1$ and $\mathbf{k}_2$ (TRa1) and $\mathbf{k}_1$ and $-\mathbf{k}_2$ (TRa2). Hereafter we adopt the classification of the patterns suggested by the authors of Ref. [34] with the only exception for AR-R (which is referred to as wavy rolls 1 in the cited paper).

The rest of the patterns are the following hexagonal ones:

(vii) Oscillating triangles (OT), $A_1 = B_1 = C_1 \neq 0$, $A_2 = B_2 = C_2 = 0$.

(viii) Standing hexagons (SH), $A_1 = A_2 = B_1 = B_2 = C_1 = C_2$.

(ix) Standing regular triangles (SRT), $A_1 = -A_2 = B_1 = -B_2 = C_1 = -C_2$.

(x) Twisted rectangles (TwR), $A_1 = A_2 = e^{i2\pi/3}B_1 = e^{i2\pi/3}B_2 = e^{-i2\pi/3}C_1 = e^{-i2\pi/3}C_2$.

(xi) Wavy rolls 2 (WR2) $A_1 = -A_2 = e^{i2\pi/3}B_1 = -e^{i2\pi/3}B_2 = e^{-i2\pi/3}C_1 = -e^{-i2\pi/3}C_2$.

Of course, there also exist SCR on a rhombic lattice that were missed by the authors of Ref. [33], but this pattern is always unstable [32]. It also should be noted that stability properties within each pair, {SH and SRT} and {TwR and WR2} cannot be distinguished in the framework of Eqs. (45) owing to their degeneracy; quintic nonlinearities are needed for that purpose.

The results on pattern selection, obtained using Ref. [33] (a misprint in the stability condition for TwR and WR2 in Ref. [33] is corrected in Ref. [34]), are presented in Fig. 7. The dashed line corresponding to $K_{0r} = 0$ is obviously the same as in Fig. 6; below this line TR are supercritical. However, for a hexagonal lattice there appears a competition between TR and TRa2. The latter pattern is stable in the domain marked with "TRa2." The entire domain of supercritical bifurcation becomes smaller because TRa2 can bifurcate either supercritically or subcritically. Moreover, as it is clear from Fig. 7(b), inverse Hopf bifurcation takes place for SRa and SH and SRT in a small domain.

We also studied competition between the oscillatory patterns on square and hexagonal lattices. This analysis demonstrates that stability domains for TR and TRa2 remain as they are shown in Fig. 7, whereas the stability domain for AR, Fig. 6(b), almost disappears. We assume that AR are unstable with respect to "external" perturbations of the

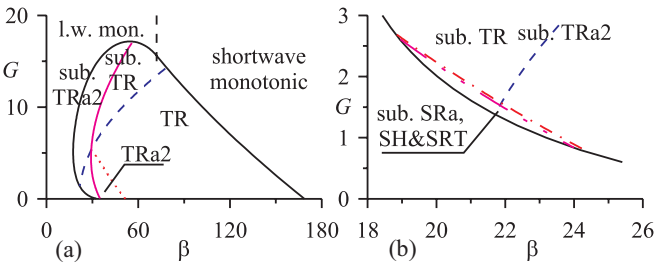

FIG. 7. (Color online) Selection of oscillatory patterns on a hexagonal lattice. (a) Domains of stability for TR (below the dashed line and to the right of the dotted line) and TRa2 (between the dotted and the solid line) are marked by "TR" and "TRa2," respectively. Above the dashed line TR bifurcates subcritically, to the left of the solid line TRa2 is subcritical. (b) Fragment of panel (a): domains of subcritical excitation for SRa and SH & SRT are situated below the dashed-double-dotted and dashed-dotted lines, respectively.

critical wave number, which do not belong to any lattice [i.e., perturbations with $\mathbf{k} = k(\cos\phi, \sin\phi)$ at arbitrary ϕ]. However, this hypothesis has not been checked.

The results for the oscillatory mode are in qualitative agreement with the nonlinear behavior found in Refs. [24,25] for similar sets of the amplitude equations. Indeed, in the cited papers stable oscillatory states with the deformed surface were found within the weakly nonlinear approach [24] and in numerical simulations [25].

V. FINITE-AMPLITUDE TWO-DIMENSIONAL REGIMES

A. Steady rolls

As was demonstrated in Sec. IV, rolls are unstable in the laterally infinite layer with respect to hexagon emergence. (The only exception is the vicinity of a dashed-dotted line in Fig. 5.) However, an analysis of 1D solutions of Eqs. (9) and (11) is of interest, for example, in the context of the layer of finite length in the y direction. In terms of the rescaled coordinate Y this means that the corresponding longitudinal size is small and thus the solution does not depend on Y.

Periodic boundary conditions are applied along the X axis. For a steady state, such boundary conditions also describe solutions in a confined layer with adiabatic vertical boundaries at $X = 0$ and $X = nL$, where $L = \pi/k$ and n is any natural number. Indeed, conditions $h_X = \theta_X = 0$ at the vertical boundaries correspond to impermeable boundaries according to Eq. (8)[3]. Hereafter we discuss both situations together, unless the opposite is stated. It is noteworthy that by providing the same steady-state solutions, these two situations are completely different in the context of the stability properties of these solutions, as discussed below.

We perform two types of calculations. The first one is a direct numerical solution of partial differential equations, Eqs. (9) and (11), for the 1D case. The method allows

[3]To satisfy the no-slip conditions one has to introduce "boundary layers" (of a thickness comparable to H) near the vertical walls, where the lubrication approximation is not valid.

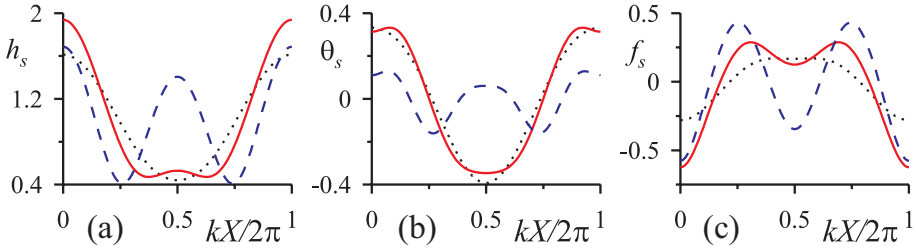

FIG. 8. (Color online) (a) Film profile, (b) variation of θ_s, and (c) $f_s = \theta_s - h_s$ with X for rolls at $\beta = 4$, $G = 1$, and $k = 1.5$. Dotted, solid, and dashed lines correspond to $M = 6$,7, and 8, respectively. The mean parts of θ_s and f_s, $\hat{\theta}_0$ and $\hat{f}_0$, are eliminated.

us to trace the nonlinear dynamics and, in particular, the relaxation processes. Of course, a stable solution of a fixed period is attained by means of this method unless some artificial symmetry of initial conditions is imposed. A faster method deals with the steady-state solution $h = h_s(X)$ and $\theta = \theta_s(X)$, which solves the boundary-value problem for ordinary differential equations. Expanding h_s and θ_s in the Fourier series

$$(h_s,\theta_s) = \sum_{n=-\infty}^{\infty} (\hat{h}_n,\hat{\theta}_n)e^{iknX};\ \hat{h}_0 = 1, \tag{46}$$

we obtain a set of nonlinear algebraic equations for the Fourier amplitudes. To ensure real values of h, one has to set $\hat{h}_n = \hat{h}^*_{-n}$ and $\hat{\theta}_n = \hat{\theta}^*_{-n}$. Moreover, due to the problem symmetry we can choose real-valued coefficients $\hat{h}_n$ and $\hat{\theta}_n$. In the numerical calculations the series were truncated at $|n| = N_m$, where N_m was chosen to guarantee the convergence of results. Depending on M and a regime under consideration, $20 < N_m < 100$ is sufficient to that end.

The typical results of calculations are presented in Figs. 8 and 9. In particular, these figures serve to describe why the finite-amplitude solution can be stable in contrast to the case of the substrate of ideal thermal conductivity [18]. In Ref. [18], the local decrease in the film thickness leads to the increase in the surface temperature and hence the decrease in the surface tension. This, in turn, increases the convective mass flux along the surface and therefore increases the initial surface distortion. There is no mechanism to saturate this process. In contrast, there is such a mechanism in the case of a substrate of low thermal conductivity. Here a local decrease in the film height does not change the heat flux from the surface considerably, whereas the heat diffusivity decreases, see the first term at the right-hand side of Eq. (11). Therefore θ_s also decreases in such a way to produce the local temperature of the free surface $f_s = \theta_s - h_s$ [or the surface tension $-f_s$, see Eq. (9)] almost constant near the hollow [cf. Figs. 8(a) and 8(c)]. This leads to a displacement of the flow from this region, which is clearly seen in Fig. 9. Moreover, increasing the Marangoni number

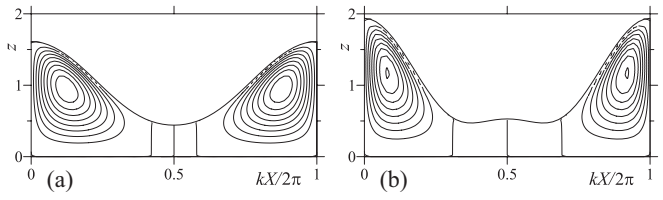

FIG. 9. Streamlines of the convective flow for rolls at $\beta = 4$, $G = 1$, and $k = 1.5$; (a) $M = 6$ and (b) $M = 7$. The step between isolines is 0.02 in panel (a) and 0.1 in panel (b).

results in a surface hump (and thus a local maximum of the surface tension) at $X = L$ and the emergence of two vortices with the opposite circulation. (The intensity of these flows is too low to be shown in Fig. 9, but the three almost vertical streamlines in the central part of this figure correspond to the boundaries of the vortices.)

The above-mentioned transformation of the minimum of $h_s(X)$ at $X = L$ to a local maximum [see the solid line in Fig. 8(a)] results in the splitting of the lower line in Fig. 10(a) into a pair of lines. With a further increase in M the surface deviation at $X = L$ grows and approaches the global maximum at $M = M_{1/2}(k)$, hence at this value of the Marangoni number the inverse period-doubling bifurcation takes place. Indeed, passing through $M_{1/2}$ from the side of the larger M, one can see that the spatial period of the solution doubles $L \to 2L$. (The subscript $1/2$ indicates that the period of the solution becomes two times smaller when M increases.)

For the parameters used in Figs. 8 and 10, $M_{1/2}(k) \approx 8.025$ [see Fig. 10(a)]. The solution of a wave number $2k$ is not shown in Fig. 8 since it is obviously unstable with respect to periodic perturbations. Moreover, the $2L$-periodic solution is also unstable at M close to (but less than) $M_{1/2}$. Indeed, on one hand, the L-periodic solution at $M > M_{1/2}$ and the $2L$-periodic one at $M < M_{1/2}$ both have (locally) an equal number of unstable eigenvalues. On the other hand, the former solution has at least one unstable eigenvalue since it bifurcates from the base state subcritically.

To confirm this conjecture, one has to explore the stability properties of steady rolls. To that end we substitute the

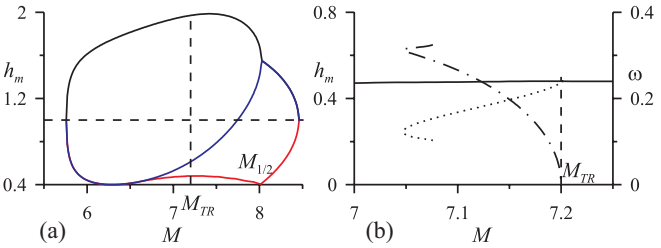

FIG. 10. (Color online) Amplitude curves for the steady rolls at $\beta = 4$, $G = 1$, and $k = 1.5$. (a) Variation of the maximum and minimum film thicknesses and $h(X = L)$ with M. Horizontal dashed line shows the thickness of the unperturbed layer, vertical line is the stability boundary $M = M_{\rm TR}$; solutions at larger M are unstable; (b) Fragment of panel (a) in the vicinity of $M = M_{\rm TR}$. Left axis is the minimum thickness of the film (solid line is the steady rolls, dotted line the TR); right axis is the frequency of the TR (dashed-dotted line).

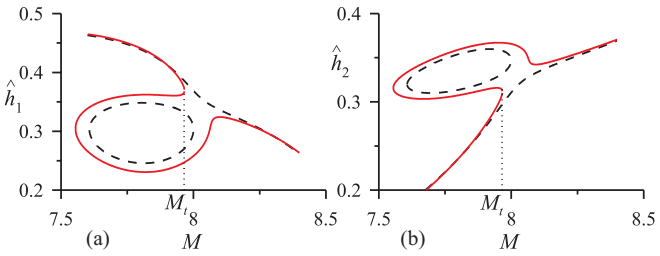

FIG. 11. (Color online) Variation of the (a) first and (b) second Fourier coefficients with the Marangoni number at $\beta = 4$, $G = 1$; $k = 1.795$ (dashed-dotted line) and $k = 1.8$ (solid line). Vertical dotted lines mark the saddle-node bifurcation at $M = M_t(k)$.

perturbed fields $h = h_s + \xi$ and $\theta = \theta_s + \vartheta$ into Eqs. (9) and (11) and linearize them with respect to the perturbations

$$\Lambda\xi = J', \tag{47}$$

$$\Lambda h_s\left(F + \frac{5}{8}\xi\right) = (h_s\vartheta' + \xi\theta_s')' - h_s'\xi' + J\left(f_s' + \frac{3}{8}h_s'\right) - \beta F - \frac{M}{48}\left(h_s^3F' + 3h_s^2f_s'\xi\right)', \tag{48}$$

$$J = \frac{h_s^3}{3}(G\xi - \xi'')' + \frac{Mh_s}{2}(h_sF' + 2f_s'\xi).$$

Here $F = \vartheta - \xi$, Λ is the growth rate, and the prime denotes the X derivative.

Assuming $2L$-periodic perturbations, we apply the Fourier transformation, reducing Eqs. (47) and (48) to a generalized algebraic eigenvalue problem

$$A\psi = \Lambda B\psi, \tag{49}$$

where ψ comprises Fourier harmonics $\hat{\xi}_n$ and $\hat{\vartheta}_n$, A and B are matrices of order $(4N_m + 1) \times (4N_m + 1)$. (Note that $\hat{\xi}_0 = 0$). This eigenvalue problem was solved numerically.

In fact, the linear stability problems for the infinite and confined layers are different. In the former case, the spectrum of wave numbers is continuous and a more general analysis should be performed on the basis of the Floquet-Bloch theory, which lies beyond the scope of the present paper. For the confined layer, the spectrum of wave numbers is discrete. Moreover, some types of periodic perturbations do not obey the impermeability condition at $X = 0, nL$ and thus they are prohibited for the confined layer. Therefore, the stability regions presented below are overestimated (only a structural stability is guarantied) for the periodic solutions and underestimated for the confined geometry.

The conjecture concerning the instability of steady rolls near $M = M_{1/2}$ is confirmed numerically; at $M > M_{\mathrm{TR}}(k)$, indicated in Fig. 10(a) by the vertical dashed line, steady rolls become unstable. At this point TR of vanishing frequency branch subcritically from steady rolls, as shown in Fig. 10(b). Of course, there exist two counter-propagating TRs, which do not possess the reflection symmetry $h(X) = h(2L - X)$; this transformation switches from one to another TR in the pair. This symmetry breakdown can be described by means of an appropriate order parameter (e.g., $\int_0^L [\xi(X) - \xi(2L - X)]\,dX$), which varies with M qualitatively similar to the waves' frequency ω, see Fig. 10(b). Such a bifurcation was found and studied in detail by the authors of Refs. [35–37].

At larger values of the wave number, as demonstrated in Fig. 11, a two-sided bifurcation takes place: With the increase in k, a double bifurcation point emerges (two branches of solution intersect), and then is destroyed, giving birth to a pair of saddle-node (tangent) bifurcations [38]. The first saddle-node bifurcation for $k > 1.797$ occurs at $M = M_t(k)$, see Fig. 11 (the subscript "t" stands for "tangent"); it is clear that the hysteretic transition takes place as M exceeds M_t. It is worth noting that the steady states shown in Fig. 11 have at least four unstable eigenvalues, therefore the "bubble-like" branch of a solution is always unstable. This is the reason why we do not discuss other branches of the Ssteady rolls any further.

The summary of calculations for $\beta = 4$, $G = 1$ is presented in Fig. 12(a). Note that both the dashed-dotted and double-dotted lines intersect the marginal stability curve at the point k_* determined by the condition

$$M_m(k_*) = M_m(2k_*).$$

This coincidence is expected for $M_{1/2}(k)$ since both the branching small-amplitude solution with given $k < k_*$ and the base state are unstable with respect to perturbations with $2k$. Indeed, at $k \approx k_*$ one obtains $M_{1/2}(k) \approx M_m(k_*) + 2M_m'(2k_*)(k - k_*)$, where the prime denotes the kth derivative of $M_m(k)$ [i.e., $M_{1/2}(k)$ locally coincides with the oblate neutral stability curve $M_m(k/2)$ at $k \approx 2k_*$]. The result for M_{TR} is less evident, but it also can be confirmed by an analytical solution, which provides $M_{\mathrm{TR}} \approx M_m(k_*) + [(V_1 - V_2)/(\gamma_1 - \gamma_2)](k - k_*)$, where $V_{1,2} = \partial\lambda/\partial k$ and $\gamma_{1,2} = \partial\lambda/\partial M$ at $M = M_m(k_*)$ and k equals either k_* or $2k_*$.

Another important feature is the transition from direct to inverse pitchfork bifurcation at $k = 1.622$, which means that K_0, which enters into Eq. (29), vanishes. At larger values of the wave number bistability takes place: both the base state and the upper branch of the steady rolls can be approached by the appropriate choice of the initial conditions.

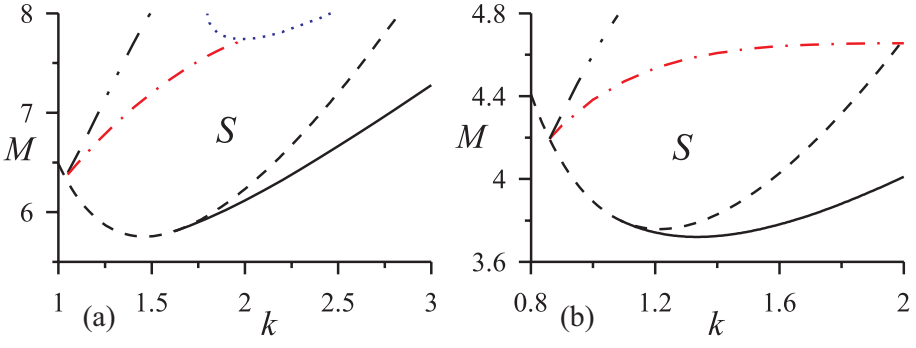

FIG. 12. (Color online) Domains of stability for steady rolls at $G = 1$; (a) $\beta = 4$ and (b) $\beta = 2$. Dashed lines are the neutral stability curves, Eq. (15); solid lines show domains of subcriticality; bistability takes place between these two lines. Dashed-dotted lines demonstrate the locus of $M_{\mathrm{TR}}(k)$, the dotted line of $M_t(k)$, and the double-dotted line of $M_{1/2}(k)$. Domains of stability are marked with "S."

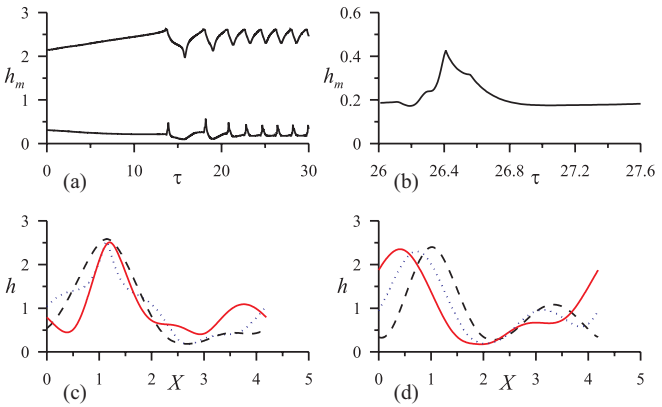

FIG. 13. (Color online) Evolution of the layer thickness; $\beta = 4, G = 1, k = 1.5, M = 7.15$. (a) Evolution of the maximum and minimum thicknesses of the film in time. (b) A zoomed in fragment of panel (a) is depicted. (c) Shape of the film at $\tau = 26, 26.2, 26.4$: dashed, dotted, and solid lines, respectively. (d) Shape of the film at $\tau = 26.6, 26.8, 27$: dashed, dotted, and solid lines, respectively.

Note that at $k > k_1 \approx 2.025$, steady rolls remain stable up to $M = M_t(k)$, and the dashed-dotted line continues on the lower (structurally unstable) branch of the bubble-like region. Thus, the later solution and even the upper branch remain unstable and they are not shown in Fig. 12(a).

In Fig. 12(b) we demonstrate the similar stability map for $\beta = 2$, when according to Fig. 4 subcritical bifurcation takes place for the regime with $k = k_c^{(m)}$. Nevertheless, the growth of disturbances does not lead to a rupture, and there exist stable 1D patterns with the deformed interface.

Our direct numerical computations show that above the stability threshold $M = M_{\mathrm{TR}}(k)$ either $2k$ rolls emerge or irregular oscillation of a strong film deformation occurs. Moreover, the irregular regime can be excited even at $M < M_{\mathrm{TR}}(k)$ by appropriate initial distortion of the film. An example of this situation is demonstrated in Fig. 13. It is clear that the evolution of the film thickness is complicated; at a part of the period the solution resembles TR, see Fig. 13(d).

B. Traveling rolls

Another regime, which can be readily studied within the 1D problem, is nonlinear traveling rolls (TR). For this solution the film thickness can be represented as follows:

$$(h_o, \theta_o) = \sum_{n=-\infty}^{\infty} (\hat{h}_n, \hat{\theta}_n) e^{ikn\eta}; \quad \hat{h}_0 = 1, \tag{50}$$

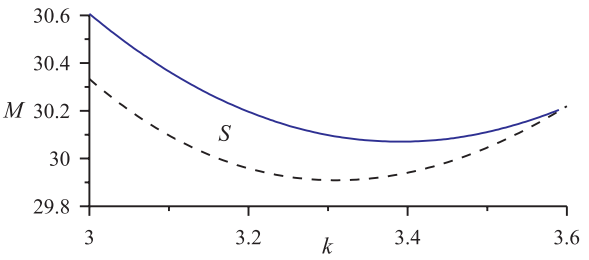

FIG. 15. (Color online) Stability region for TR (marked with "S") for $\beta = 40$, $G = 5$. Dashed line is the marginal stability curve $M_o(k)$; solid line shows $M_{\mathrm{SR}}(k)$. Above this line TR are unstable with respect to perturbations of the same period.

with $\eta = X - V\tau$, where $V = \omega k$ is yet unknown phase velocity of the wave. Of course, for TR there is no reflection symmetry (inversion of the coordinate X obviously changes the sign of V as well). Thus the coefficients $\hat{h}_n$ are now complex; the only restriction imposed on $\hat{h}_n$ is $\hat{h}_n = \hat{h}^*_{-n}$, which ensures that h is real.

The results of calculations for TR are presented in Figs. 14 and 15. It is clear from the former figure that both the deflection of the free surface and the temperature perturbation considerably grow with the increase in M, whereas the profile of $f_o = \theta_o - h_o$ steepens quickly. This growth of the derivative seems to be an origin of the instability of TR. Although the branch of the solution corresponding to TR can be obtained at large enough values of M, TR become unstable at $M = M_{\mathrm{SR}}$, which is close to the marginal stability curve, see Fig. 15.

Above this stability threshold we have found nontrivial dynamics when the system rambles between two unstable limit cycles, TR and standing roll (SR), being alternatively attracted to and then repelled from each of them, see Fig. 16. Of course, such dynamics is impossible within the simplest amplitude equation, Eq. (43). Indeed, it is evident from Fig. 16 that the instability of TR is caused by the perturbation with the derivative close to discontinuity [see solid line in Fig. 16(c)]. Such a mode is obviously lost when a reduction to the central manifold is performed and therefore only several lower Fourier harmonics are accounted for.

The formation of a pattern close to SR, in turn, takes place only within a very short time period, marked by the vertical dashed lines in Fig. 16(b); the corresponding snapshots of the film surface are presented in Fig. 16(d). Moreover, as is clear from this panel, the solution is not a perfect SR since the slow drift of the structure along the X axis still exists. This property has a simple explanation. Since $M_{\mathrm{SR}}(k)$ is rather close to $M_o(k)$, the instability of SR and the transition to TR can be approximately described by Eq. (43). The corresponding

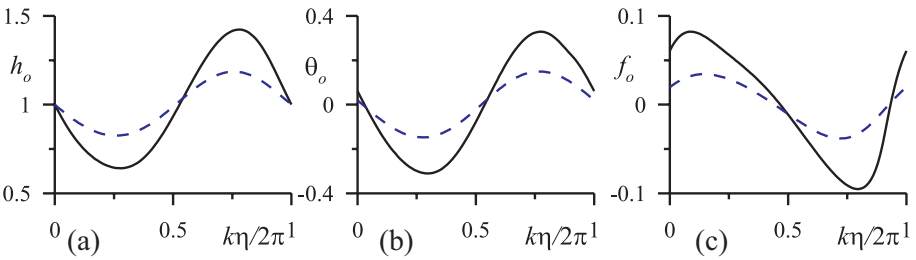

FIG. 14. (Color online) (a) The film thickness $h_o(\eta)$, (b) the main part of the temperature $\theta_o(\eta)$, and (c) $f_o = \theta_o - h_o$ for TR at $\beta = 40$, $G = 5$, $k = 3.3$. Dashed (solid) lines correspond to $M = 30$ ($M = 30.4$). The mean parts of the temperature ($\hat{\theta}_0$) and the surface tension ($\hat{f}_0$) have been dropped.

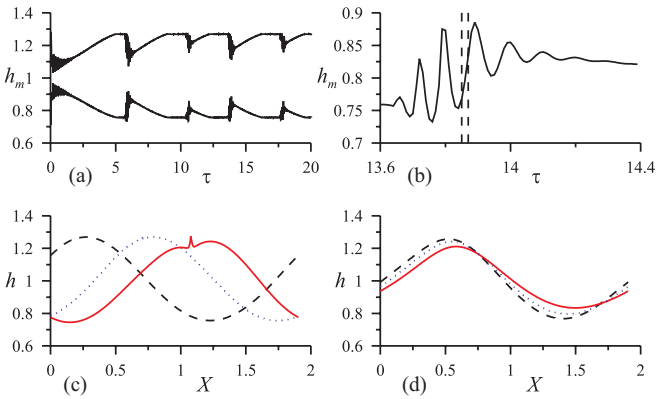

FIG. 16. (Color online) Evolution of the layer thickness above the stability threshold for TR; $\beta = 40, G = 5, M = 30.11, k = 3.3$. (a) Evolution of the maximum and minimum thicknesses of the film in time; panel (b) depicts a zoomed-in fragment of panel (a). (c) Formation of TR and the initial stage of its instability; shape of the film at $\tau = 12.5, 13, 13.7$, the dashed, dotted, and solid lines, respectively. (d) Formation and instability of the state close to SR; shape of the film at $\tau = 13.85, 13.86, 13.87$, the dashed, dotted, and solid lines, respectively. [This time interval is marked by vertical dashed lines in panel (b).]

growth rate is large enough; it is proportional to $M - M_o(k)$, in contrast to the growth rate for the TR, which is proportional to $M - M_{\mathrm{SR}}$. Of course, the smallness of the latter growth rate ensures that the heteroclinic cycle TR $\rightarrow$ SR $\rightarrow$ TR is attracting (at least at M close to M_{SR}) according to the criterion formulated in Ref. [39].

VI. CONCLUSION AND DISCUSSION

In this paper we consider the classical problem: a Marangoni convection in a layer heated from below with a deformable free surface. Using unusual scaling, $K = O(\sqrt{\mathrm{Bi}})$, and the more frequently used condition $\mathrm{Ca} \gg 1$ such that the product $\beta = \mathrm{BiCa}$ remains finite, we derive a novel set of amplitude equations, Eqs. (9) and (11), which describe a coupled evolution of the film height and the primary (averaged across the layer) part of the temperature.

This set of equations is reminiscent of the amplitude equations derived by the authors of Refs. [24,25], but here such equations are derived for a simpler physical system. As far as the comparison, first, the amplitude functions in all three works are qualitatively similar: the layer thickness h and the primary part of the temperature (or the concentration in Ref. [24]). Second, the capillary number is effectively large, which involves the regularizing term with higher (fourth) spatial derivatives.

Having h as one of the amplitude functions distinguishes these problems from other systems where a long-wave oscillatory mode exists (e.g., a convection in a binary mixture [40,41]). Indeed, the amplitude equations governing the nonlinear dynamics should include h, whereas for the convection in a binary mixture the contributions are only from the nonlinear combinations of the *gradients* of the amplitude functions (the leading parts of the temperature and concentration).

Another important distinction manifests itself even within the linear stability problem. In Refs. [26,27,40,41] all the linear terms bear either second space or first temporal derivatives and thus the dispersion relation is quadratic in the wave number. In contrast, the above-mentioned surface-tension term (the fourth space derivative) results in a more complicated dispersion relation, see Refs. [24,25] and Eq. (19) in the present paper. (In our case there also exists the derivatives-free term, which describes the heat loss from the free surface.)

Linear stability analysis within this set demonstrates the emergence of the monotonic and oscillatory modes; the corresponding expressions for the neutral stability curves are given by Eqs. (21) and (22). The oscillatory mode was not found in prior studies of Marangoni convection when heating is from below.

Weakly nonlinear analysis carried out within the set of the amplitude equations shows that supercritical excitation is possible for both steady and oscillatory convection. Depending on the problem parameters, either hexagons or rolls can be selected in the steady case, whereas among the oscillatory patterns either traveling rolls or traveling rectangles are stable. Stable states with a deformed free surface is a very rare occurrence, which was earlier found by the authors of Refs. [24,25] or for weak surface deformations [12,20]. Another remarkable feature is the stability of rolls against squares, which was earlier found only for finite values of the Biot number [31].

Finally, we perform numerical calculations of regular steady and traveling rolls in the simplest one-dimensional $(1 + 1)$ case: the space-periodic solutions and their stability are studied. (We deal only with the structural stability, i.e., stability with respect to perturbations of the same spatial period.) A complicated sequence of bifurcations is found for periodic steady solutions. Traveling rolls are structurally stable only within a thin band near the marginal stability curve, see Fig. 15.

ACKNOWLEDGMENTS

We are grateful to A. A. Nepomnyashchy and A. Oron for the fruitful discussions. A.A. acknowledges President's Grant No. MK-22368.2011.1. M.K. acknowledges the support of WKU Faculty Scholarship Council via Grants No. 10-7016 and No. 10-7054.

[1] J. R. A. Pearson, J. Fluid Mech. **4**, 489 (1958).
[2] L. E. Scriven and C. V. Sternling, J. Fluid Mech. **19**, 321 (1964).
[3] K. A. Smith, Fluid Mech. **24**, 401 (1966).
[4] S. H. Davis, Annu. Rev. Fluid Mech. **19**, 403 (1987).
[5] P. Colinet, J.-C. Legros, and M. G. Velarde, *Nonlinear Dynamics of Surface-Tension-Driven Instabilities* (Wiley-VCH, Berlin, 2001).

[6] A. A. Nepomnyashchy, M. G. Velarde, and P. Colinet, *Interfacial Phenomena and Convection* (Chapman and Hall/CRC Press, London, 2001).
[7] R. V. Birikh, V. A. Briskman, M. G. Velarde, and J.-C. Legros, *Liquid Interfacial Systems. Oscillations and Instability* (Marsel Dekker, New York, 2003).
[8] M. Takashima, J. Phys. Soc. Jpn. **50**, 2751 (1981).
[9] R. V. Birikh, V. A. Briskman, R. N. Rudakov, and M. G. Velarde, Int. J. Heat Mass Transfer **38**, 2723 (1995).
[10] E. Knobloch, Physica D **41**, 450 (1990).
[11] L. Shtilman and G. Sivashinsky, Physica D **52**, 477 (1991).
[12] A. A. Golovin, A. A. Nepomnyashchy, and L. M. Pismen, Physica D **81**, 117 (1995).
[13] A. Oron, S. H. Davis, and S. G. Bankoff, Rev. Mod. Phys. **69**, 931 (1997).
[14] R. V. Craster and O. K. Matar, Rev. Mod. Phys. **81**, 1131 (2009).
[15] S. Krishnamoorthy, S. B. Ramaswamy, and S. W. Joo, Phys. Fluids **7**, 2291 (1995).
[16] A. Oron, Phys. Fluids **12**, 1633 (2000).
[17] L. Y. Yeo, R. V. Craster, and O. K. Matar, Phys. Rev. E **67**, 056315 (2003).
[18] S. J. VanHook, M. F. Schatz, J. B. Swift, W. D. McCormick, and H. L. Swinney, J. Fluid Mech. **345**, 45 (1997).
[19] S. Shklyaev, A. V. Straube, and A. Pikovsky, Phys. Rev. E **82**, 020601(R) (2010).
[20] P. L. Garcia-Ybarra, J. L. Castillo, and M. G. Velarde, Phys. Fluids **30**, 2655 (1987).
[21] A. Podolny, A. Oron, and A. A. Nepomnyashchy, Phys. Fluids **17**, 104104 (2005).
[22] S. Shklyaev, A. A. Nepomnyashchy, and A. Oron, Phys. Fluids **21**, 054101 (2009).
[23] S. Shklyaev, M. Khenner, and A. A. Alabuzhev, Phys. Rev. E **82**, 025302(R) (2010).
[24] A. Podolny, A. Oron, and A. A. Nepomnyashchy, Phys. Fluids **18**, 054104 (2006).
[25] T. P. Lyubimova, D. V. Lyubimov, Y. Parshakova, and A. Ivantsov, Micrograv. Sci. Technol. **23**, 143 (2011).
[26] T. P. Lyubimova and Y. N. Parshakova, Fluid Dyn. **42**, 695 (2007).
[27] Y. N. Parshakova, Ph.D. thesis, Institute of Continuous Media Mechanics UB RAS, Perm, Russia, 2008 (in Russian).
[28] R. B. Hoyle, *Pattern Formation: An Introduction to Methods* (Cambridge University Press, Cambridge, England, 2006).
[29] E. Buzano and M. Golubitsky, Philos. Trans. R. Soc. London A **308**, 617 (1983).
[30] M. Golubitsky, J. W. Swift, and E. Knobloch, Physica D **10**, 249 (1984).
[31] M. Bestehorn, Phys. Rev. E **48**, 3622 (1993).
[32] M. Silber and E. Knobloch, Nonlinearity **4**, 1063 (1991).
[33] M. Roberts, J. W. Swift, and D. H. Wagner, Contemp. Math. **56**, 283 (1986).
[34] T. Clune and E. Knobloch, Physica D **74**, 151 (1994).
[35] P. Coullet, R. E. Goldstein, and G. H. Gunaratne, Phys. Rev. Lett. **63**, 1954 (1989).
[36] S. Fauve, S. Douady, and O. Thual, J. Phys. (France) II **1**, 311 (1991).
[37] W. Barten, M. Lücke, M. Kamps, and R. Schmitz, Phys. Rev. E **51**, 5636 (1995).
[38] G. Iooss and D. D. Joseph, *Elementary Stability and Bifurcation Theory* (Springer, New York, 1989).
[39] I. Melbourne, P. Chossat, and M. Golubitsky, Proc. R. Soc. Edinburgh, A **113**, 315 (1989).
[40] L. M. Pismen, Phys. Rev. A **38**, 2564 (1988).
[41] A. Oron and A. A. Nepomnyashchy, Phys. Rev. E **69**, 016313 (2004).